Biosensors and Bioelectronics 139 (2019) 111332

Contents lists available at ScienceDirect

Biosensors and Bioelectronics

journal homepage: www.elsevier.com/locate/bios

Quantitative differential monitoring of the metabolic activity of *Corynebacterium glutamicum* cultures utilizing a light-addressable potentiometric sensor system

Shahriar Dantism[a,c], Désirée Röhlen[a], Thorsten Selmer[a], Torsten Wagner[a,b], Patrick Wagner[c], Michael J. Schöning[a,b,*]

[a] Institute of Nano- and Biotechnologies (INB), Aachen University of Applied Sciences, Campus Jülich, 52428, Jülich, Germany
[b] Institute of Complex Systems (ICS-8), Research Centre Jülich GmbH, 52425, Jülich, Germany
[c] Department of Physics and Astronomy, Soft-Matter Physics and Biophysics Section, KU Leuven, Celestijnenlaan 200 D, 3001, Leuven, Belgium

ARTICLE INFO

Keywords:
Light-addressable potentiometric sensor (LAPS)
Corynebacterium glutamicum
Metabolic activity
Living cell number
Differential measurement
3D-printed multi-chamber set-up

ABSTRACT

Applying biosensors for evaluation of the extracellular acidification of microorganisms in various biotechnological fermentation processes is on demand. An early stage detection of disturbances in the production line would avoid costly interventions related to metabolically inactive microorganisms. Furthermore, the determination of the number of living cells through cell plating procedure after cultivations is known as time- and material-consuming. In this work, a differential light-addressable potentiometric sensor (LAPS) system was developed to monitor the metabolic activity of *Corynebacterium glutamicum* (*C. glutamicum* ATCC13032) as typical microorganism in fermentation processes. In this context, the number of living cells in suspensions was directly determined utilizing the read-out principle of the LAPS system. The planar sensor surface of the LAPS design allows to fixate 3D-printed multi-chamber structures, which enables differential measurements. In this way, undesirable external influences such as pH variations of the medium and sensor signal drift can be compensated.

1. Introduction

Early-stage detection of possible inhibition factors within fermentation processes is significant to avoid costly and time-consuming interventions at different stages in industrial bio-production. Especially, in the presence of disturbances related to metabolically inactive microorganisms, the performance of a bioreactor will decline and the production chain can get blocked. In this context, on-line monitoring of the metabolic activity of cells (O'Mara et al., 2018; Reinecke et al., 2017; Simons et al., 2017; Qiu et al., 2014) or bacteria (Buchenauer et al., 2009; Qiu et al., 2014; Marquard et al., 2017) is crucial and should be considered. A biogas fermentation process is an appropriate example for monitoring such process workflows (Ahring, 2003). A few examples for the wide range of such applications include monitoring of CO_2 and CH_4 concentrations in a biogas matrix from different biomass structures (Selvaraj et al., 2017), low-cost digester monitoring under realistic conditions (Castro et al., 2017), monitoring of a biogas process during pulse loads with ammonia (Bruni et al., 2013), and monitoring of microbial communities in anaerobic digestion sludge for biogas optimization (Lim et al., 2018). At the same time, a comprehensive analysis of the cellular metabolism of bacteria inside fermenters is a complex task due to the variety of involved microorganisms in different steps of the biogas fermentation process (hydrolysis, acidogenesis, acetogenesis and methanogenesis). The process itself might be seen as a kind of a "black box". At the input stage, the fermenter is fed with biomass (*e.g.*, crops, corn silage, manure). The amount and the quality of different end products (*e.g.*, CH_4, H_2O and CO_2) can be evaluated with well-known methods and devices at the output stage (Havukainen et al., 2014). One approach to study the cellular metabolism of bacteria in biofermentation processes is to use test microorganisms such as *Escherichia coli*, *Corynebacterium glutamicum*, *Lactobacillus lactis*, and *Lactobacillus brevis*. In the present work, we have selected *C. glutamicum* ATCC13032 as a Gram-positive, rod-shaped, non-motile, non-pathogenic soil bacterium, which was originally isolated in Japan to identify glutamate production in 1956 (Kinoshita et al., 1957). It is moreover employed in the production of large-scale industrial amino acids such as L-glutamate, L-lysine (Liebl, 2005; Udaka, 2008), L-serine, L-tryptophan, L-isoleucine, L-phenylalanine, and L-valine (Sprenger, 2007; Pàtek, 2007; Stolz et al., 2007). Correspondingly, on-line monitoring of the extracellular acidification of *C. glutamicum* can enable a better

* Corresponding author. Institute of Nano- and Biotechnologies (INB), Aachen University of Applied Sciences, Campus Jülich, 52428, Jülich, Germany.
E-mail address: schoening@fh-aachen.de (M.J. Schöning).

https://doi.org/10.1016/j.bios.2019.111332
Received 28 February 2019; Received in revised form 29 April 2019; Accepted 15 May 2019
Available online 21 May 2019
0956-5663/

control of amino acid production in industrial processes. Referring to a biogas fermentation process and with knowledge about the metabolic activity of these microorganisms, different process states of a biogas reactor can be analyzed and monitored in real-time. To achieve this, it is important to establish the correlation between the status of the bioreactor and the output signal of the sensor, which reflects the metabolic state of the microorganism. This way, a mapping of the fermentation process can be developed for an early-stage detection, which can avoid unwanted process crashes.

Here, field-effect biosensors can play an important role and are commonly used sensor systems applied for various monitoring applications (Bergveld, 1996). Detection of acetoin and penicillin (Molinnus et al., 2018; Poghossian et al., 2018), ultrasensitive detection of DNA (Mei et al., 2018), label-free detection of allergens in food (Hideshima et al., 2018), and detection of heart failure-related biomarkers in whole blood (Lei et al., 2017) are some current examples for the use of field-effect biosensors. The principle of field-effect biosensors distinguishes between three types of sensor systems: i) ion-selective field-effect transistors (ISFET); ii) electrolyte/insulator/semiconductor (EIS) structures; and (iii) light-addressable potentiometric sensors (LAPS). In comparison with ISFET, the LAPS chip manufacturing (see Section 2.1), miniaturization, encapsulation, and handling are relatively straightforward. The read-out principle of EIS structures can get rather complex in terms of multivariate data analysis when using array-type arrangements. Due to movable or multi-light pointers, typically used in the LAPS set-up, concentration changes of (bio-)chemical species in the analyte solution can be detected in a spatially resolved way on its planar sensor surface (Hafeman et al., 1988; Yoshinobu et al., 2005, 2015; Dantism et al., 2018).

In this work, a differential measurement set-up based on the read-out principle of a LAPS system is utilized to determine the metabolic activity of *C. glutamicum* after glucose uptake. Usually, counting the number of viable cells is performed with cell-plating procedures considering the number of "Colony Forming Units" (CFU/mL) or by using expensive high-throughput cell-plating technologies (*e.g.*, ROTOR HAD, SINGER Instruments) in specialized analytical laboratories. In the new approach, the LAPS set-up can be used for both the determination of the metabolic activity of *C. glutamicum* and also for counting the number of living cells through their metabolic activity. The main goals in the present work are, therefore: 1) monitoring of the extracellular acidification of *C. glutamicum* after glucose uptake by means of a differential LAPS system; 2) introducing a method to determine the number of living cells directly through their cellular metabolism on the LAPS and finding a correlation between the number of living cells and the LAPS signal response. Note here that only living cells in *C. glutamicum* suspensions can display a metabolic activity, which is in turn the basis for the output of a bioreactor.

2. Material and methods

2.1. Microfabrication and electrochemical characterization of LAPS chips

The LAPS chip is based on a p-doped ⟨100⟩ silicon wafer with a thickness of 540 µm and a specific electrical resistivity of 5–10 Ωcm. A thin insulator layer (30 nm) of SiO_2 was prepared by means of a thermal dry oxidation procedure (40 min at 1000 °C, O_2). On top of the insulator layer, 30 nm of Tantalum (Ta) was grown applying an electron-beam evaporation process (0.5 nm/s, at 6×10^{-6} mbar). An additional thermal dry oxidation step (45 min at 520 °C, O_2) was utilized to oxidize the Ta and to create this way a highly pH-sensitive transducer layer (60 nm, Ta_2O_5) (Schöning et al., 2005a,b; Poghossian et al., 1992). The metallization of the Ohmic rear-side contact (Al, 300 nm) was achieved with a final electron-beam evaporation step at 2 nm/s. After dicing the silicon wafer into single chips of 20 mm × 20 mm size, a part of the rear-side of each chip was removed using a wet-chemical etching process with 5% hydrofluoric acid (HF). This way, an active sensor area of 15 mm × 15 mm was defined for the rear-side illumination. Fig. 1 illustrates the LAPS chip and its layers. After fabrication, well-known electrochemical characterization methods were employed to characterize the sensor behaviour such as capacitance-voltage (C–V), photocurrent-voltage (I–V), impedance spectroscopy, leakage-current measurements, and constant-capacitance (ConCap) measurements (Poghossian et al., 2004). The pH sensitivity of the sensor was determined by applying different Titrisol buffer concentrations (1 mL of pH 3, 5, 7, 9 and 11, respectively) (Dantism et al., 2018). In LAPS measurements, 200 µL of the buffer solution were filled in each chamber ($volume_{max}$/chamber = 1 mL). For all control measurements, an electrochemical spectrum analyzer (Zahner-Elektrik GmbH) and a Ag/AgCl reference electrode (Metrohm GmbH) were used.

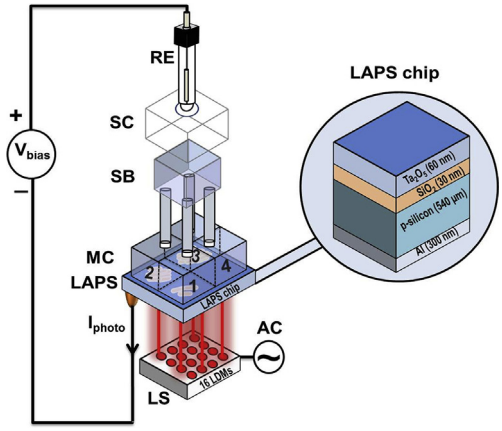

Fig. 1. Schematic illustration of the four-chamber differential measurement system based on LAPS principle. RE: Ag/AgCl reference electrode, SC: sealing cap, SB: salt bridge chamber, MC: multi-chamber structure fixed on the sensor surface. The LAPS is consisting of an Al/p-Si/SiO_2/Ta_2O_5 layer structure and a modulated light source (LS) based on 16 laser-diode modules; 1–3: active sensor chambers with cells; 4: reference sensor chamber without cells; I_{photo}: photocurrent; V_{bias}: bias voltage; AC: alternating current; LDMs: laser-diode modules.

2.2. Read-out principle of LAPS

The LAPS read-out principle can be shortly described, as follows: by supplying a DC (Direct Current) bias voltage (V_{bias}) across the sensor structure through a Ag/AgCl reference electrode in contact with the analyte solution, a space-charge region at the insulator/semiconductor interface will be formed. A modulated rear-side illumination unit based on 16 small-sized fixed-focus tunable infrared laser-diode modules (LDMs, λ = 785 nm, Roithner Lasertechnik GmbH, Vienna, Austria, serial number APCD-780-07-C3) have been used to generate electron-hole pairs inside the silicon substrate (Fig. 1). The laser-diode modules (LDMs) were simultaneously modulated with a base frequency of 1 kHz utilizing a field-programmable gate array (FPGA)-based microcontroller. More information about the illumination unit and the FPGA-based microcontroller can be found in the references (Dantism et al., 2018; Werner et al., 2011, Engström and Carlsson, 1983).

The charge carriers are separated in the created electrical field of the space-charge region enabling a photocurrent (I_{photo}) depending on the surface potential, with an alternating amplitude (for more details, see also (Schöning et al., 2005a,b; Yoshinobu et al., 2015). Since the pH-sensitive transducer layer (Ta_2O_5) of the LAPS chip is in direct contact with the analyte solution containing the microorganisms, changes in the surface potential can occur due to the extracellular acidification of microorganisms. The operation of a LAPS chip can be modeled for illuminated and non-illuminated areas by means of an equivalent circuit diagram, which is explained in detail in ref. (Poghossian et al., 2017).

2.3. Differential LAPS set-up

In order to eliminate undesired external influences during measurements (*e.g.*, pH variations of the medium, temperature fluctuations or sensor signal drifts), a differential LAPS measurement set-up was constructed with 3D-printed multi-chambers. All chambers are photopolymer-based (PP-ABS: polypropylene-acrylonitrile-butadiene-styrene) and were printed by means of an UV-LED 3D-printer (Freeform Pico Plus27, Asiga) (Dantism et al., 2016). In such arrangement, one chamber (chamber 4) serves as the reference chamber without cells, whereas all other chambers (chambers 1, 2, 3) function as active sensor sites with cells. By substracting the data for the reference chamber from the values obtained for the cell-loaded, active chambers, the differential signal can be calculated. For addressing all chambers with the same V_{bias} and reducing the number of the Ag/AgCl reference electrodes in multi-chamber LAPS measurements, a 3D-printed (PP-ABS) salt-bridge chamber (1 mL of 3 M KCl) was developed and combined with a sealing cap to avoid evaporation of the inner electrolyte. More information about the size, geometry, and characteristics of all developed 3D-printed structures incorporated with the LAPS system can be found in Dantism et al. (2018).

3. Results and discussion

3.1. Four-chamber differential LAPS measurements with C. glutamicum and glucose

Metabolically active acid-forming microorganisms in suspensions will increase the H^+-ion activity on the sensor surface after uptaking glucose. An increase of the H^+-ion activity causes a potential shift on the LAPS surface. The cellular response mechanism and the average acidification rates for cells in general are discussed in literature, see *e.g.*, (Owicki and Parce, 1992; Werner et al., 2012). By plotting these potential changes versus time, a drop of the sensor signal can be observed after adding *C. glutamicum* cells to chambers together with glucose. Fig. 2 exemplary depicts the mean values of potential changes (in mV) *vs.* time collected from four consecutive independent measurements with glucose concentrations from 0.17 mM to 1.67 mM and three different cell numbers from 1.2×10^9 cells to 4.8×10^9 cells. The first measurement was carried out with the lowest glucose concentration of 0.17 mM. The sensor chip was conditioned with the glucose solution for 10 min. After the conditioning phase, cells were added. Recorded signals are indicated with red, green and blue lines for three different cell numbers, respectively. The black line represents the LAPS signal response from the reference sensor side without cells only containing PBS. Considering the fact that in chamber 4 no cells were available, the signal remains stable, as expected and described in literature (Dantism et al., 2018). In chambers with cells (chambers 1, 2, 3), all recorded signals were dropping due to the metabolically induced pH shift on the sensor surface of the LAPS after the acidification phase of *C. glutamicum*. A potential change of approx. 10 mV was measured by the lowest cell number of 1.2×10^9 cells in the chamber 1 (red line). In chamber 2 with 2.4×10^9 cells a potential change value of approx. 16 mV was recorded. In chamber 3 (blue line) with the highest cell number (4.8×10^9 cells), the highest potential change value of approx. 20 mV was observed. After finishing the first set of measurements (40 min), the sensor surface was washed several times with PBS solution (pH 7.4, 0.2 mM) and the next glucose concentration (0.33 mM, pH 7.4) was loaded. The same measurement procedure was performed for further glucose concentrations (0.5 mM and 1.67 mM). Note, for the last set of measurements at 1.67 mM glucose concentration, a potential signal drop of approx. 82 mV was determined at the highest cell number (blue line). Considering a pH sensitivity of the LAPS with Ta_2O_5 as pH-sensitive transducer material of 54 mV/pH (Dantism et al., 2018), for such experimental condition a signal drop of 82 mV corresponds to a pH change at the interface "cells/LAPS surface" of $\Delta pH \approx 1.5$. Consequently, the original pH value of 7.4 is decreased at the interface to pH 5.9, also influencing the metabolic activity of the cells, which can be seen by the flattening of the sensor signal. Respectively, in the first chamber with the lowest cell number, a signal drop of approx. 53 mV and for the second highest cell number a decrease of approx. 69 mV were recorded. In accordance with published results for *E. coli* bacteria in (Dantism et al., 2016, 2017, 2018), the higher the glucose concentration or the cell number in the respective chamber, the higher potential changes can be expected.

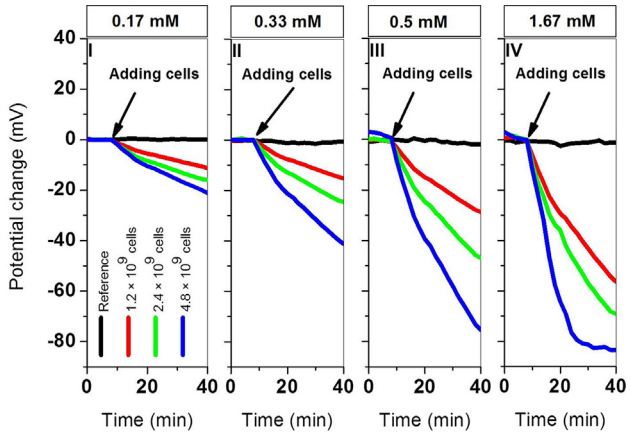

Fig. 2. Four-chamber differential LAPS measurement with varying cell number of *C. glutamicum* (1.2×10^9, 2.4×10^9, 4.8×10^9 cells in 200 µL cell suspension) and varying glucose concentration (0.17 mM, 0.33 mM, 0.5 mM, 1.67 mM). Potential changes of four successive independent measurements with an ascending row of glucose concentrations. Black line: reference sensor side without cells; red, green and blue lines: active sensor sides with cells. Four LDMs were considered for each chamber (each curve corresponds to calculated mean values). (For interpretation of the references to colour in this figure legend, the reader is referred to the Web version of this article.)

For the performed experiments, the data with its associated 3D plot are overviewed in Fig. 3a, b, where the potential change rate (PCR) is defined as slope of the dropped sensor signal in the linear range after adding cells. Here, after a conditioning phase of the sensor signal for 10 min with glucose solutions, the PCR values were calculated from the slope of the sensor signal for the first 6 min after adding cells (see arrows in Fig. 2) to the respective chambers. The highest PCR value of (4.9 ± 0.04) mV/min was achieved by 4.8×10^9 cells and 1.67 mM glucose. In addition, the lowest PCR value of (0.6 ± 0.03) mV/min was obtained by 1.2×10^9 cells and 0.17 mM glucose (Fig. 3a and b). Furthermore, the PCR values increase systematically with increasing glucose concentration and/or cell number. It should be noted that the increase of the sensor signal due to the cellular metabolism displays a non-linear behaviour. Moreover, a saturated sensor signal behaviour was observed. This effect will be explained in Section 3.2 in more detail.

By means of the developed multi-chamber differential LAPS system, the metabolic activity of *C. glutamicum* has successfully been monitored for different cell numbers and glucose concentrations. With the help of the 4-chamber set-up, two varying parameters in the analyte solution (cell number and glucose concentration) can be simultaneously monitored with regard to the reference signal, thus eliminating possible drift effects of the sensor signal. The evaluated PCR values with their corresponding cell numbers and glucose concentrations were applied as a calibration matrix allowing to determine unknown number of living cells in the following section.

3.2. Correlation between the number of living cells and the LAPS signal

Fig. 4 depicts the correlation between mean PCR values and living cell numbers at a constant glucose concentration of 1.67 mM. In the diagram, the three measurement points with red arrows represent the

a)

Glucose C (mM)	N Cells/200 µL	|Potential change rate| (mV/min)
0.17	1.2×10^9	0.6 ± 0.03
	2.4×10^9	0.8 ± 0.01
	4.8×10^9	1.1 ± 0.02
0.33	1.2×10^9	0.8 ± 0.04
	2.4×10^9	1.2 ± 0.06
	4.8×10^9	2.0 ± 0.09
0.5	1.2×10^9	1.3 ± 0.05
	2.4×10^9	2.1 ± 0.09
	4.8×10^9	3.5 ± 0.15
1.67	1.2×10^9	2.1 ± 0.11
	2.4×10^9	3.1 ± 0.22
	4.8×10^9	4.9 ± 0.04

b)

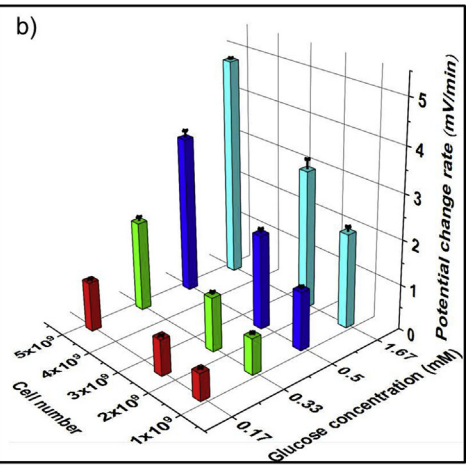

Fig. 3. Mean values and standard deviations of potential change rates for four successive measurements with different glucose concentrations (0.17 mM, 0.33 mM, 0.5 mM, 1.67 mM) when varying cell numbers (1.2×10^9, 2.4×10^9, 4.8×10^9 cells) in 200 µL cell suspension. Data are calculated from Fig. 2 and summarized in **a)**. 3D plot of potential change rates for all different cell numbers and glucose concentrations, **b)**. The error bars indicate the variation from the mean values of three independent LAPS measurements applying four measurement spots for each chamber. Mean values and standard deviations of potential change rates were obtained from three independent measurement repetitions in an interval of 6 min after adding cells.

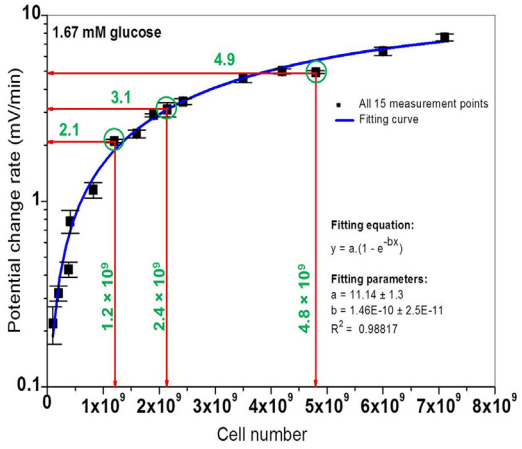

Fig. 4. Correlation between living cell number and LAPS signal response. Mean values of potential change rates for fifteen successive measurements with different cell numbers in 200 µL cell suspension, when varying the cell number at a constant glucose concentration of 1.67 mM. Three measurement points with red arrows and marked green circles were obtained from Fig. 3 at 1.67 mM glucose. Blue line: exponential fitting curve for all fifteen measurement points following a Michaelis-Menten kinetics. The error bars indicate the variation from the mean values of three independent LAPS measurements applying four measurement spots for each measurement chamber. (For interpretation of the references to colour in this figure legend, the reader is referred to the Web version of this article.)

results from the calibration matrix in Fig. 3 for 1.67 mM glucose. For the experiment, 12 additional cell numbers (1×10^8, 2×10^8, 3.8×10^8, 4.1×10^8, 8.2×10^8, 1.6×10^9, 1.9×10^9, 2.3×10^9, 3.5×10^9, 4.2×10^9, 6.0×10^9, and 7.1×10^9 cells) have been studied in terms of their metabolic activity marked also as black measurement spots. The blue line illustrates the exponential fitting curve related to all 15 measurement points: by increasing the number of living cells, the PCR values increase systematically. The fitted correlation curve follows the Michaelis-Menten saturation kinetics, which is exemplarily described in more detail for cell-based biosensors in Huck et al. (2013). Here, an increase of the number of cells during the measurement, or blockades of glucose uptakes by higher glucose concentrations or cell numbers on the sensor surface results in a saturation behaviour and no further increase of the sensor signal. Among the black points, for instance, the highest cell number of 7.1×10^9 cells correlates with the highest sensor signal response at (7.6 ± 0.33) mV/min. Respectively, the lowest signal response of (0.22 ± 0.10) mV/min represents to the lowest counted cell number of 1×10^8 cells.

Furthermore, to determine the "unknown" cell numbers N in a bacterial suspension through their metabolic activity on the sensor surface, additional LAPS measurements were performed at a constant glucose concentration of 1.67 mM. Three different cell numbers (1 N, 0.5 N, and 0.25 N) were used in this experiment. Before adding cell suspensions (200 µL), the sensor surface of each chamber was conditioned with 100 µL of the glucose solution (pH 7.4) for 10 min. The lowest cell number of 0.25 N was pipetted to chamber 1. Consequently, 0.5 N cells were added to chamber 2. The highest cell number 1 N (suspension without dilution with PBS) was loaded to chamber 3. Fig. 5, exemplarily depicts the differential signal responses (potential changes) with the LAPS set-up. These potential changes can be seen as green triangles, red dots and black squares. From these potential changes, the mean values and standard deviations of potential change rates (PCR) for three independent measurements were calculated 6 min after adding cells (black arrow in Fig. 5) in 200 µL suspension at a constant glucose concentration (1.67 mM). The calculated PCR values can be summarized as: the black measurement points (chamber 1) with 0.25 N cells represent the lowest potential drop of approx. 21 mV, which corresponds to a potential change rate of (0.78 ± 0.10) mV/min; the red points belong to chamber 2 with 0.5 N cells and a potential drop of approx. 38 mV, that is a potential change rate of (1.15 ± 0.11); the highest potential drop of approx. 64 mV was observed in chamber 3 with 1 N cells (green points), corresponding to a potential change rate of (2.30 ± 0.11) mV/min. For higher cell numbers, higher potential

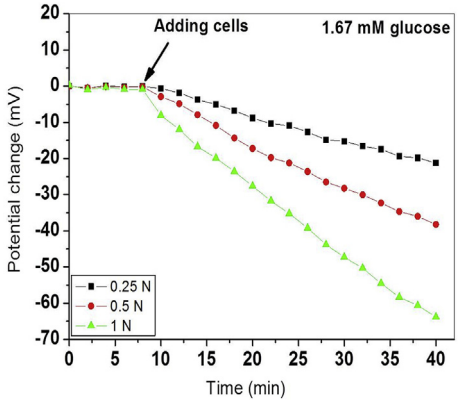

Fig. 5. Differential LAPS signals exemplarily shown after substracting the data of the reference chamber without cells from the particular potential change values of the active chambers with cells at a fixed glucose concentration of 1.67 mM with "unknown" cell numbers N. The black line with 0.25 N cells represents the lowest cell number in contrast to the green line with 1 N cells as the highest cell number. The red measurement points represent the cell number of 0.5 N cells. (For interpretation of the references to colour in this figure legend, the reader is referred to the Web version of this article.)

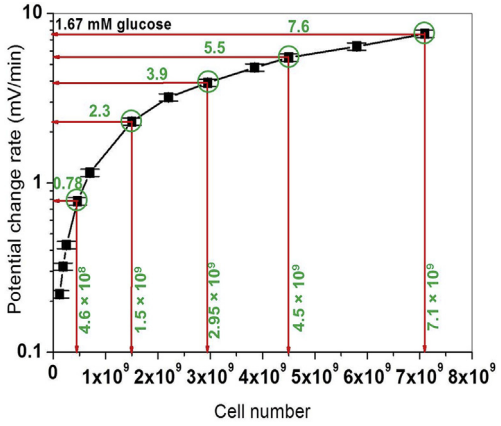

Fig. 6. Correlation between living cell number and LAPS signal response for measurements with "unknown" cell numbers. Mean values of potential change rates for twelve successive measurements with different cell numbers in 200 µL cell suspension are marked in black. The glucose concentration of 1.67 mM was kept constant. Five cell numbers were exemplarily selected for comparison with cell plating procedures, which are marked by red arrows and green circles. The error bars indicate the variation from the mean values of three independent LAPS measurements applying four measurement spots for each measurement chamber. (For interpretation of the references to colour in this figure legend, the reader is referred to the Web version of this article.)

changes were recorded due to an increase of the cellular metabolism on the sensor surface, as expected.

The same procedure was applied to determine the PCR values of further "unknown" cell numbers (in total 12). By means of calculating the PCR values and comparing these with the plotted calibration curve from Fig. 4, the number of living cells can be graphically evaluated. Here, the intersection points of the calibration curve with the particular PCR values can be selected to obtain the number of cells on the x-axis. Fig. 6 illustrates the correlation between the PCR values and living cell numbers obtained from Figs. 4 and 5. The highest cell number of 7.1×10^9 cell was read at a potential-change rate of (7.6 ± 0.33) mV/min. At a PCR value of (0.22 ± 0.05) mV/min, the lowest cell number of 1.2×10^8 cells was determined. Basing on this calibration plot, the "unknown" cell number N from Fig. 5 can be determined as $N = 1.5 \times 10^9$ cells.

In order to compare the cell numbers achieved from LAPS-based measurements with the counted cells through a conventional cell plating procedure, five cell numbers (evaluated by LAPS) were exemplarily selected (green-marked circles in Fig. 6), as follows: 4.6×10^8, 1.5×10^9, 2.95×10^9, 4.5×10^9, and 7.1×10^9 cells. These cell numbers were compared to cell numbers determined with the viable plate counting procedure with the respective suspensions and have been: 4.0×10^8, 1.2×10^9, 2.8×10^9, 4.2×10^9, and 6.8×10^9 cells in 200 µL. Comparing the cell numbers by these two methods, a good correlation could be achieved. Slightly lower cell numbers were determined after the cell plating procedure. The reason might be related to some inaccuracies in the cell plating procedure itself, for instance, during the serial dilution steps for cell growing on agar plates. Nonetheless, the method of determination of the number of living cells in suspensions through their metabolic activity with the help of LAPS can be used as a reliable, fast, inexpensive, and highly promising measurement procedure.

4. Conclusion and outlook

The read-out principle of a LAPS system was utilized to monitor for the first time the cellular metabolism of bacteria of *C. glutamicum*. Cell-based experiments were performed with a four-chamber differential LAPS set-up with three known cell numbers (1.2×10^9, 2.4×10^9, 4.8×10^9 cells) and four glucose concentrations (0.17, 0.33, 0.5, 1.67 mM) simultaneously. It was shown that by increasing the cell number or glucose concentration, PCR values were also increased due to an increase of the cellular metabolism on top of the sensor surface. The highest PCR value of (4.9 ± 0.04) mV/min was achieved by 4.8×10^9 cells and 1.67 mM glucose. The lowest PCR value of (0.6 ± 0.03) mV/min was obtained by 1.2×10^9 cells and 0.17 mM glucose. Furthermore, the "unknown" number of living cells was monitored by LAPS through their metabolic activity. Here, cell numbers between 7.1×10^9 cells with a PCR of (7.6 ± 0.38) mV/min and 1.2×10^8 with a PCR of (0.22 ± 0.05) mV/min were recorded. Five cell numbers were selected to be compared with counted cell numbers after cell plating procedure as a reference method. A good correlation between both methods underlines the advantages of LAPS for the determination of the number of living cells in suspensions showing reproducible and reliable results. At the same time, the LAPS method is fast and inexpensive. In future experiments, the metabolic activity of further test microorganisms will be determined by means of the developed differential multi-chamber LAPS set-up. Here, a simultaneous multivariate analysis of the cellular metabolism of different microorganisms is envisaged. In this way, a calibration database can be build up with the studied microorganisms. Subsequently, cell-based measurements with real samples from different biogas process stages should be performed. It should be demonstrated how the fermentation solution will influence the cellular metabolism of different microorganisms. In the next step and in relation to the values in the calibration database, the signal changes might serve as control parameters to monitor and to steer the biogas process.

CRediT authorship contribution statement

Shahriar Dantism: Writing - original draft, Writing - review & editing, Visualization, Data curation. **Désirée Röhlen:** Methodology. **Thorsten Selmer:** Methodology. **Torsten Wagner:** Formal analysis. **Patrick Wagner:** Supervision, Validation, Writing - review & editing. **Michael J. Schöning:** Supervision, Validation, Writing - review & editing.

Acknowledgements

The authors thank the German Federal Ministry of Food and Agriculture (project no.: 22006613) and the German Federal Ministry of Education and Research (project no.: 13N12585) for the financial support of this work. Moreover, we would like to thank H. Iken for the LAPS chip processing, and B. Schneider for the 3D-printed structures.

Appendix A. Supplementary data

Supplementary data to this article can be found online at https://doi.org/10.1016/j.bios.2019.111332.

References

Ahring, B.K., 2003. Biomethanation I. Springer, Berlin, Heidelberg, pp. 1–30.
Buchenauer, A., Hofmann, M.C., Funke, M., Büchs, J., Mokwa, W., Schnakenberg, U., 2009. Biosens. Bioelectron. 24 (5), 1411–1416.
Bruni, E., Ward, A.J., Køcks, M., Feilberg, A., Peter, A., Adamsen, S., Jensen, A.P., Poulsen, A.K., 2013. Biomass Bioenergy 56, 211–220.
Bergveld, P., 1996. Sens. Actuators, A 56, 65–73.
Castro, L., Escalante, H., Jaimes-Estévez, J., Diaz, L.J., Vecino, K., Rojas, G., Mantilla, L., 2017. Bioresour. Technol. 239, 311–317.
Dantism, S., Röhlen, D., Wagner, T., Wagner, P., Schöning, M.J., 2018. Phys. Status Solidi 215 (15), 1–8 1800058.
Dantism, S., Takenaga, S., Wagner, P., Wagner, T., Schöning, M.J., 2016. Phys. Status Solidi 213 (6), 1479–1485.
Dantism, S., Takenaga, S., Wagner, T., Wagner, P., Schöning, M.J., 2017. Electrochim. Acta 246, 234–241.
Engström, O., Carlsson, A., 1983. J. Appl. Phys. 54, 5245–5251.
Havukainen, J., Uusitalo, V., Niskanen, A., Kapustina, V., Horttanainen, M., 2014. Renew.

Energy 66, 232–240.
Hideshima, S., Saito, M., Fujita, K., Harada, Y., Tsuna, M., Sekiguchi, S., Kuroiwa, S., Nakanishi, T., Osaka, T., 2018. Sens. Actuators, B 254, 1011–1016.
Hafeman, D.G., Parce, J.W., McConnell, H.M., 1988. Science 240, 1182–1185.
Huck, C., Schiffels, J., Herrera, N.C., Schelden, M., Selmer, T., Poghossian, A., Baumann, M., Wagner, P., Schöning, M.J., 2013. Phys. Status Solidi 210 (5), 926–931.
Kinoshita, S., Udaka, S., Shimono, M., 1957. J. Gen. Appl. Microbiol. 3, 193–205.
Lim, J.W., Ge, T., Tong, Y.W., 2018. Waste Manag. 71, 334–341.
Liebl, W., 2005. *Corynebacterium* taxonomy. In: Eggeling, L., Bott, M. (Eds.), Handbook of *Corynebacterium Glutamicum*. CRC, Boca Raton, pp. 9–34.
Lei, Y.M., Xiao, M.M., Li, Y.T., Xu, L., Zhang, H., Zhang, H.Y., Zhang, G.J., 2017. Biosens. Bioelectron. 91, 1–7.
Marquard, D., Schneider-Barthold, C., Düsterloh, S., Scheper, T., Lindner, P., 2017. J. Biotechnol. 259, 83–85.
Molinnus, D., Muschallik, L., Gonzalez, L.O., Bongaerts, J., Wagner, T., Selmer, T., Siegert, P., Keusgen, M., Schöning, M.J., 2018. Biosens. Bioelectron. 115, 1–6.
Mei, J., Li, Y.T., Zhang, H., Xiao, M.M., Ning, Y., Zhang, Z.Y., Zhang, G.J., 2018. Biosens. Bioelectron. 110, 71–77.
O'Mara, P., Farrell, A., Bones, J., Twomey, K., 2018. Talanta 176, 130–139.
Owicki, J.C., Parce, J.W., 1992. Biosens. Bioelectron. 7 (4), 255–272.
Pàtek, M., 2007. Branched chain amino acids. In: Wendisch, V.F. (Ed.), Amino Acid Biosynthesis-Pathway, Regulation and Metabolic Engineering. Springer, Heidelberg, pp. 129–162.
Poghossian, A., Jablonski, M., Koch, C., Bronder, T.S., Rolka, D., Wege, C., Schöning, M.J., 2018. Biosens. Bioelectron. 110, 168–174.
Poghossian, A.S., Jablonski, M., Koch, C., Bronder, T.S., Wege, C., Schöning, M.J., 1992. Sens. Actuators, B 7 (1–3), 367–370.
Poghossian, A., Mai, D.T., Mourzina, Y., Schöning, M.J., 2004. Sens. Actuators, B 103 (1–2), 423–428.
Poghossian, A., Werner, C.F., Buniatyan, V.V., Wagner, T., Miyamoto, K., Yoshinobu, T., Schöning, M.J., 2017. Sens. Actuators, B 244, 1071–1079.
Qiu, J., Arnold, M.A., Murhammer, D.W., 2014. J. Biotechnol. 173, 106–111.
Reinecke, T., Biechele, P., Sobocinski, M., Suhr, H., Bakes, K., Solle, D., Jantunen, H., Scheper, T., Zimmermann, S., 2017. Sens. Actuators, B 251, 1009–1017.
Simons, A.D., Williams III, C., Degoix, A., Sikavitsas, V.I., 2017. Biosens. Bioelectron. 90, 443–449.
Selvaraj, R., Abdul Nasir, K.T., Vasa, N.J., Shiva Nagendra, S.M., 2017. Sens. Actuators, A 249, 378–385.
Sprenger, G.A., 2007. Aromatic amino acids. In: Wendisch, V.F. (Ed.), Amino Acid Biosynthesis-Pathway, Regulation and Metabolic Engineering. Springer, Heidelberg, pp. 93–127.
Stolz, M., Peters-Wendisch, P., Etterich, H., Gerharz, T., Faurie, R., Sahm, H., Feresterra, H., Eggeling, L., 2007. Appl. Environ. Microbiol. 73, 750–755.
Schöning, M.J., Brinkmann, D., Rolka, D., Demuth, C., Poghossian, A., 2005a. Sens. Actuators, B 111–112, 423–429.
Schöning, M.J., Wagner, T., Wang, C., Otto, R., Yoshinobu, T., 2005b. Sens. Actuators, B 108 (1–2), 808–814.
Udaka, S., 2008. The discovery of *Corynebacterium glutamicum* and birth of amino acid fermentation industry in Japan. In: Burkovski, A. (Ed.), *Corynebacteria*: Genomics and Molecular Biology. Caister Academic, Norfolk, pp. 1–6.
Werner, C.F., Schusser, S., Spelthahn, H., Wagner, T., Yoshinobu, T., Schöning, M.J., 2011. Electrochim. Acta 56 (26), 9656–9660.
Werner, C.F., Groebel, S., Krumbe, C., Wagner, T., Selmer, T., Yoshinobu, T., Baumann, E.M., Keusgen, M., Schöning, M.J., 2012. Phys. Status Solidi 209, 900–904.
Yoshinobu, T., Miyamoto, K.I., Wagner, T., Schöning, M.J., 2015. Sens. Actuators, B 207, 926–932.
Yoshinobu, T., Iwasaki, H., Ui, Y., Furuichi, K., Ermolenko, Yu, Mourzina, Yu, Wagner, T., Näther, N., Schöning, M.J., 2005. Methods 37, 94–102.